A Marie-Curie-ITN
within H2020

Proceedings of the International Symposium on
Thermal Effects in Gas flows In Microscale
October 24-25, 2019 – Ettlingen, Germany

ISTEGIM 2019 - 276530

INVESTIGATION OF MIXED CONVECTION IN A VERTICAL MICROANNULUS: VISCOUS DISSIPATION EFFECT

Ayse Nur Altunkaya[*1], Mete Avci[2], Orhan Aydin[2]
[*1]Department of Mechanical Engineering, Recep Tayyip Erdogan University,
53100 Rize, Turkey
aysenur.altunkaya@erdogan.edu.tr
[2]Department of Mechanical Engineering, Karadeniz Technical University,
61080 Trabzon, Turkey
mavci@ktu.edu.tr, oaydin@ktu.edu.tr

KEY WORDS

Slip flow regime, mixed convection, viscous dissipation, vertical microannulus.

ABSTRACT

In this study, problem of mixed convection in a vertical microannulus subjected to uniform heat flux thermal boundary condition is investigated theoretically. The analysis is carried out in a form which includes both the effects of viscous dissipation (Br) and rarefaction (Kn) at fully developed laminar flow condition. By taking into account slip flow regime, first order slip velocity and temperature jump boundary conditions are applied to governing equations. A semi-analytical method, the perturbation method, is used to solve the momentum and the energy governing equations. For different values of radius ratio (r), the effects of mixed convection parameter (Gr/Re), viscous dissipation (Br), and rarefaction (Kn) on the velocity and temperature distributions and Nusselt number are discussed. It is disclosed that the increase in the value of Gr/Re increases the Nusselt number on both inner and outer walls while an opposite trend is obtained with an increase in the value of Br or r*.*

1. INTRODUCTION

Advances in the field of manufacturing techniques have given a great acceleration to the fabrication of micro-scale electromechanical systems (MEMS), which offer superior performances compared to macro-scale systems. Fundamental studies have shown that some effects and conditions (e.g., rarefaction, viscous dissipation or slip-flow) that are normally neglected in macro-scale convection can alter the fluid flow and heat transfer characteristics significantly at micro-scale. Although many earlier studies focused on forced convection in micro-scales, the studies regarding natural or mixed convection are limited.

The natural convection problem in an open-ended vertical parallel plate microchannel was first studied by Chen and Weng [1] for the asymmetric wall temperature boundary condition. The effects of rarefaction and fluid-wall interaction were found to increase the volume flow and to decrease the heat transfer rate. They also analyzed the natural convection problem in a vertical annular microchannel for different curvature radius ratios, rarefaction and accommodation coefficients (momentum and thermal accommodation coefficients) [2]. Haddad et al. [3] numerically investigated the natural convection in a vertical parallel-plate microchannel in the slip flow regime $(10^{-3} \le Kn \le 10^{-1})$. Their results emphasized the significant effect of rarefaction on the temperature distribution and Nusselt number. The entrance effect for natural convection in a vertical microchannels was numerically considered by Biswall et al. [4]. Their results showed that the increase in the Rayleigh and the Knudsen numbers increased the Nusselt number. Sadeghi et al. [5] applied the second law of thermodynamics to annular microchannel geometry for the fully developed flow condition by taking the viscous heating and first order boundary conditions into account. Natural convection in an open-ended vertical parallel-plate microchannel including the second-order slip model, thermal creep effect and variable

[*] Corresponding author

thermophysical properties was studied by Rahimi and Niazmand [6]. It was found that the second-order effects reduced the temperature jump and slip velocity, whereas the thermal creep strongly increased the slip velocity in both developing and fully developed regions. Jha et al. [7] investigated the effect of magnetic field on fluid velocity, volumetric flow rate and skin friction inside a vertical microannulus for both hydrodynamically and thermally fully developed conditions. It was determined that the fluid velocity and the volume flow rate decreased with an increase in the magnetic field.

Mixed convection in some common microgeometries was firstly investigated by our research group [8-10]. Avci and Aydin [8-9] analytically investigated fully developed flow in a vertical parallel-plate microchannel for the asymmetric wall temperature and heat flux thermal boundary conditions in the slip flow regime. In another study, Avci and Aydin [10] analytically investigated the effect of mixed convection parameter, Knudsen number and aspect ratio on the Nusselt number in a vertical microannulus for the fully developed flow condition. It was found that the Nusselt number decreased with an increase in Kn while an opposite trend is observed with an increase in the mixed convection parameter. Karimipour et al. [11] studied the gravity effects on the mixed convection heat transfer in a microchannel using the lattice Boltzman method. It was shown that the effects of buoyancy forces were important for $Kn < 0.05$ while they could be ignored $Kn > 0.05$. Mixed convection flow in an asymmetrically heated long vertical microchannel was numerically analyzed by Jian and Weng [12] for the second-order slip conditions. It was disclosed that the second-order slip had an appreciable effect on the flow but a negligible effect on the heat transfer. Sadeghi A. et al. [13] investigated the fully developed flow mixed convection in vertical microducts in the slip flow regime for different cross sections (triangle, square, hexagon, circle and rectangle). Two axially constant heat flux boundary conditions of H1 and H2 were considered in the analysis. For the triangular section channel, the Nusselt number increased and the pressure drop decreased with an increase in the mixed convection parameter. In a very similar study, Sadeghi M. et al. [14] extended their study for the vertical microducts of constant but arbitrary geometry. As a general character, they indicated that the friction resistance and Nusselt number increased with a decrease in Knudsen number. Moslehi and Saghafian [15] focused on the developing hydrodynamical and thermal behaviors of mixed convection gas flow in a vertical microplane channel under uniform magnetic field condition. Their result showed that the friction factor increased significantly with an increase in Ha. It is also found that the effect of the mixed convection parameter on the Nusselt number was negligible. Avramenko et al. [16] analytically and numerically investigated the mixed convection problem in a microtube subjected to a linear change in wall temperature. Mixed convection in a vertical microannulus including the effect of temperature dependent viscosity and slip flow regime was studied by Jha and Aina [17]. It was found that the Knudsen number reduced the rate of heat transfer, whereas the values of viscosity variation parameter increased the rate of heat transfer and skin friction.

Besides the effects of rarefaction and mixed convection parameter, viscous dissipation is an another critical effect that should be taken into consideration at microscale. Due to the high velocities in the small passages, it distorts the temperature profiles and, in the following, heat-transfer rates by playing a role as an internal heat-generation source. In our very recent article [18], we studied mixed convection in a vertical parallel-plate microchannel including the viscous dissipation effect. As an extension of that article, here, we studied the mixed convection problem in a vertical microannulus with constant heat flux boundary condition by including viscous dissipation effect into analysis. To the authors' best knowledge, this is the first study for mixed convection in this geometry considering the effects of rarefaction and viscous dissipation effects together.

2. METHOD

The schematic of the mixed convection problem in a vertical microannulus is depicted in Fig. 1. The analysis is presented in the form of a set of mathematical modeling and analysis steps. The flow is considered to be steady, laminar and fully developed both hydrodynamically and thermally. All thermophysical properties are assumed to be independent of temperature.

The microannulus is assumed to be long enough to reach the existence of a fully developed flow. In this case, the axial velocity and dimensionless temperature components and the axial pressure gradient will no longer change after a certain length along the channel ($\partial u/\partial x = 0$, $\partial \theta/\partial x = 0$ and $dp/dx = const.$). For the details, readers are referred to see Aung and Worku [19].

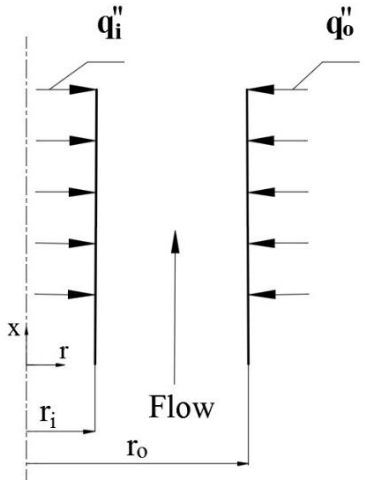

Figure 1: Schematic of the problem geometry.

Using the usual Boussinesq approximation with the aforementioned considerations, the momentum and energy equations in cylindrical coordinates can be written as in the following:

$$0 = -\frac{dp}{dx} + \frac{\mu}{r}\frac{d}{dr}\left(r\frac{du}{dr}\right) + \beta g \rho_0 \left(T - T_m\right) \tag{1}$$

$$u\frac{\partial T}{\partial x} = \alpha\left(\frac{\partial^2 T}{\partial x^2} + \frac{1}{r}\frac{\partial}{\partial r}\left(r\frac{\partial T}{\partial r}\right)\right) + \frac{\nu}{c_p}\left(\frac{du}{dr}\right)^2 \tag{2}$$

where the third terms on the right sides of Eq. (1) is the buoyancy force and the second term in the right hand side of Eq. (2) represents viscous dissipation term. The symbols appearing in the above set of equations are as follows: p is the pressure; u the axial velocity; T the temperature; g the gravitational acceleration; μ the dynamic viscosity; β the thermal expansion coefficient; ρ the density; α the thermal diffusivity; ν the kinematic viscosity and c_p the specific heat at constant pressure, respectively.

Here, T_m denotes the mean fluid temperature defined as:

$$T_m = \frac{2}{r_o^2 - r_i^2}\int_{r_i}^{r_o} T(x,r) r dr \tag{3}$$

In the fully developed flow for the corresponding boundary conditions, the local temperature has a linear variation, see Barletta and Rossi di Schio [20]. On the basis of this way; the axial temperature gradient in the fully developed region is written as:

$$\frac{\partial T}{\partial x} = \frac{dT_m}{dx} \tag{4}$$

The non-dimensional temperature distribution shows a constant change while the temperature distribution is in a continuous change in the flow direction $\left(\frac{\partial}{\partial x}\left[(T - T_m)\Big/(q_i'' D_h / k)\right] = 0\right)$. Based on this condition and taking into account the Eq. (4), Eq. (2) can be arranged as follows:

$$\frac{k}{r}\frac{\partial}{\partial r}\left(r\frac{\partial T}{\partial r}\right) + \mu\left(\frac{du}{dr}\right)^2 = \rho_0 c_p u \frac{dT_m}{dx} \tag{5}$$

In the analysis, the usual continuum approach is integrated with the two main characteristics of the microscale phenomena: the velocity slip and the temperature jump [22].

$$u_s = \frac{2 - \sigma_v}{\sigma_v}\lambda\left(\frac{\partial u}{\partial n}\right)_w \tag{6}$$

$$T_s - T_w = \frac{2-\sigma_t}{\sigma_t}\frac{2\gamma}{\gamma+1}\frac{\lambda}{\mathrm{Pr}}\left(\frac{\partial T}{\partial n}\right)_w \tag{7}$$

where σ_v and σ_t are the tangential momentum accommodation coefficient and the thermal accommodation coefficient, respectively. Their typical values (near unity) are taken in the analysis.

For the solution of Eqs. (1) and (2), the corresponding boundary conditions are written as:

$$u(r) = u_{s_i}, \quad \frac{\partial T}{\partial r} = -\frac{q_i''}{k} \quad \text{at} \quad r = r_i \tag{8a}$$

$$u(r) = u_{s_o}, \quad \frac{\partial T}{\partial r} = \frac{q_o''}{k} \quad \text{at} \quad r = r_o \tag{8b}$$

where k is the thermal conductivity, q_i'' and q_o'' are the heat fluxes at the inner and outer cylinders, respectively.

Multiplying the both sides of Eq. (5) with r and then integrating it with respect to r in the range of $[r_i, r_o]$ gives:

$$\frac{dT_m}{dx} = \frac{2}{(r_o^2 - r_i^2)u_m r_o^2 c_p \rho_0}\left[r_o q_o'' + r_i q_i'' + \mu\int_{r_i}^{r_o} r\left(\frac{du}{dr}\right)^2 dr\right] \tag{9}$$

where u_m denotes the mean velocity which can be determined from:

$$u_m = \frac{2}{r_o^2 - r_i^2}\int_{r_i}^{r_o} u(r) r dr \tag{10}$$

Substituting Eq. (9) back into Eq. (5) and Eq. (5) is rearranged as:

$$\frac{k}{r}\frac{\partial}{\partial r}\left(r\frac{\partial T}{\partial r}\right) + \mu\left(\frac{du}{dr}\right)^2 = 2\frac{u}{(r_o^2 - r_i^2)r_o^2 u_m}\left[r_o q_o'' + r_i q_i'' + \mu\int_{r_i}^{r_o} r\left(\frac{du}{dr}\right)^2 dr\right] \tag{11}$$

The dimensionless quantities described for a constant heat flux boundary condition can be written as:

$$R = \frac{r}{r_o}, \quad r^* = \frac{r_i}{r_o}, \quad U = \frac{u}{u_m}, \quad \mathrm{Re} = \frac{u_m D_h}{\nu}, \quad \theta = \frac{T - T_m}{q_i'' D_h / k}$$

$$Gr = \frac{\beta g q_i'' D_h^4}{k\nu^2}, \quad Br = \frac{\mu u_m^2}{q_i'' D_h}, \quad r_q = \frac{q_o''}{q_i''}, \quad \beta_v = \frac{2-\sigma_v}{\sigma_v}, \quad Kn = \frac{\lambda}{D_h}$$

$$\beta_t = \frac{2-\sigma_t}{\sigma_t}\frac{2\gamma}{\gamma+1}\frac{1}{\mathrm{Pr}}, \quad P = \frac{p}{\rho u_m^2}, \quad X = \frac{x}{\mathrm{Re}\, D_h}, \quad \zeta = -\frac{dP}{dX} \tag{12}$$

where $D_h (= 2(r_o - r_i))$ is the channel hydraulic diameter.

By introducing the above- nondimensional parameters, the governing equations take the following forms:

$$\frac{1}{R}\frac{d}{dR}\left(R\frac{dU}{dR}\right) = -\frac{Gr}{4(1-r^*)^2\,\mathrm{Re}}\theta - \frac{1}{4(1-r^*)^2}\zeta \tag{13}$$

$$\frac{1}{R}\frac{d}{dR}\left(R\frac{d\theta}{dR}\right) = -Br\left(\frac{dU}{dR}\right)^2 + \frac{2}{1-r^{*2}}U\left(\frac{r_q + r^*}{2(1-r^*)} + Br\eta\right) \tag{14}$$

where

$$\eta = \int_{r^*}^{1} R\left(\frac{dU}{dR}\right)^2 dR \tag{15}$$

The nondimensional boundary conditions can be rewritten as:

$$U(r^*) = 2\beta_v Kn(1-r^*)\left.\frac{dU}{dR}\right|_{R=r^*}, \quad U(1) = -2\beta_v Kn(1-r^*)\left.\frac{dU}{dR}\right|_{R=1} \tag{16}$$

$$\left.\frac{d\theta}{dR}\right|_{R=r^*} = -\frac{1}{2(1-r^*)}, \quad \left.\frac{d\theta}{dR}\right|_{R=1} = \frac{r_q}{2(1-r^*)} \tag{17}$$

In a similar manner, the dimensionless mean fluid temperature and the mean velocity given in Eqs. (3) and (10) can be arranged as:

$$\int_{r^*}^{1} \theta(R) R dR = 0 \tag{18a}$$

$$\int_{r^*}^{1} U R dR = \frac{1-r^{*2}}{2} \tag{18b}$$

When the effect of the viscous dissipation is neglected ($Br = 0$), Eqs. (13) and (14) are transformed into a linear form and an analytical solution is possible.

$$\frac{1}{R}\frac{d}{dR}\left(R\frac{dU}{dR}\right) = -\frac{Gr}{4(1-r^*)^2\,\mathrm{Re}}\theta - \frac{1}{4(1-r^*)^2}\zeta \tag{19}$$

$$\frac{1}{R}\frac{d}{dR}\left(R\frac{d\theta}{dR}\right) = U\left(\frac{r_q + r^*}{(1-r^{*2})(1-r^*)}\right) \tag{20}$$

Differentiating both sides of Eq. (19) with respect to R and substituting obtained temperature gradient into Eq. (20), one can obtained a fourth-order linear differential equation for U, as follows:

$$\frac{1}{R}\frac{d}{dR}\left\{R\frac{d}{dR}\left[\frac{1}{R}\frac{d}{dR}\left(R\frac{dU}{dR}\right)\right]\right\} = C^4 U \tag{21}$$

Similarly, the regarding boundary conditions can be rearranged as:

$$U(r^*) = 2\beta_v Kn(1-r^*)\left.\frac{dU}{dR}\right|_{R=r^*}, \quad \frac{d}{dR}\left\{\frac{1}{R}\frac{d}{dR}\left(R\frac{dU}{dR}\right)\right\} = \frac{Gr}{8\,\mathrm{Re}}\frac{1}{(1-r^*)^3} \quad \text{at} \quad R = r^* \tag{22a}$$

$$U(1) = -2\beta_v Kn(1-r^*)\left.\frac{dU}{dR}\right|_{R=1}, \quad \frac{d}{dR}\left\{\frac{1}{R}\frac{d}{dR}\left(R\frac{dU}{dR}\right)\right\} = -\frac{Gr}{8\,\mathrm{Re}}\frac{r_q}{(1-r^*)^3} \quad \text{at} \quad R = 1 \tag{22b}$$

where C is the dimensionless parameter defined as:

$$C^4 = -\frac{Gr}{4\,\mathrm{Re}}\frac{(r_q + r^*)}{(1-r^*)^4(1+r^*)} \tag{23}$$

When Eq. (18a) is taken into account and both sides of Eq. (19) are multiplied by R and then Eq. (19) is integrated with respect to R in the range of [r^*,1], the dimensionless parameter ζ can be obtained as follows:

$$\zeta = \frac{8(1-r^*)}{(1+r^*)}\left(r^*\left.\frac{dU}{dR}\right|_{R=r^*} - \left.\frac{dU}{dR}\right|_{R=1}\right) \tag{24}$$

Substituting the dimensionless velocity and Eq. (24) into Eq. (19), the dimensionless temperature profile can be obtained as:

$$\theta = -\frac{1}{\left(\frac{Gr}{4(1-r^*)^2\,\mathrm{Re}}\right)}\left[\frac{1}{R}\frac{d}{dR}\left(R\frac{dU}{dR}\right) + \frac{1}{4(1-r^*)^2}\zeta\right] \tag{25}$$

In the presence of viscous dissipation ($Br \neq 0$), the momentum and energy equations (Eqs. (13-14)) get a non-linear form, and, therefore they cannot be solved analytically. In this case, by considering (Gr/Re) as the perturbation parameter, the solution of the regarding equations can be obtained approximately by using the perturbation expansion as in the following:

$$U(R) = U_0(R) + \frac{Gr}{\mathrm{Re}}U_1(R) + \left(\frac{Gr}{\mathrm{Re}}\right)^2 U_2(R) + \cdots = \sum_{n=0}^{\infty}\left(\frac{Gr}{\mathrm{Re}}\right)^n U_n(R) \tag{26}$$

$$\theta(R) = \theta_0(R) + \frac{Gr}{\mathrm{Re}}\theta_1(R) + \left(\frac{Gr}{\mathrm{Re}}\right)^2 \theta_2(R) + \cdots = \sum_{n=0}^{\infty}\left(\frac{Gr}{\mathrm{Re}}\right)^n \theta_n(R) \tag{27}$$

$$\zeta = \zeta_0 + \frac{Gr}{\mathrm{Re}}\zeta_1 + \left(\frac{Gr}{\mathrm{Re}}\right)^2 \zeta_2 + \cdots = \sum_{n=0}^{\infty}\left(\frac{Gr}{\mathrm{Re}}\right)^n \zeta_n \tag{28}$$

$$\eta = \eta_0 + \frac{Gr}{\mathrm{Re}}\eta_1 + \left(\frac{Gr}{\mathrm{Re}}\right)^2 \eta_2 + \cdots = \sum_{n=0}^{\infty}\left(\frac{Gr}{\mathrm{Re}}\right)^n \eta_n \tag{29}$$

where Gr is the Grashof number, Re is the Reynolds number and U and θ are the dimensionless velocity and temperature, respectively.

By applying Eqs. (26-29) into Eqs. (13-14) and Eqs. (16-18), sets of ordinary differential equations can be obtained, which can be solved in succession and yield unknown functions of $U_n(R)$ and $\theta_n(R)$ and unknown parameters of ζ_n and η_n. A sequential solution procedure beginning with the zero-order problem, $n=0$, and then progressing to $n=1,2,...$ etc. is followed.

In regard to the above method, the zero order problem $(n=0)$ yields:

$$\frac{1}{R}\frac{d}{dR}\left(R\frac{dU_0}{dR}\right) = -\frac{1}{4(1-r^*)^2}\zeta_0$$

$$U_0(r^*) = 2\beta_v Kn(1-r^*)\left.\frac{dU_0}{dR}\right|_{R=r^*}, \qquad U_0(1) = -2\beta_v Kn(1-r^*)\left.\frac{dU_0}{dR}\right|_{R=1}$$

$$\int_{r^*}^{1} U_0 R dR = \frac{1-r^{*2}}{2} \tag{30}$$

$$\frac{1}{R}\frac{d}{dR}\left(R\frac{d\theta_0}{dR}\right) = -Br\left(\frac{dU_0}{dR}\right)^2 + \frac{2}{1-r^{*2}}U_0\left(\frac{r_q + r^*}{2(1-r^*)} + Br\eta_0\right)$$

$$\left.\frac{d\theta_0}{dR}\right|_{R=r^*} = -\frac{1}{2(1-r^*)}, \qquad \left.\frac{d\theta_0}{dR}\right|_{R=1} = \frac{r_q}{2(1-r^*)}$$

$$\int_{r^*}^{1} \theta_0 R dR = 0 \tag{31}$$

For the symmetric case ($r_q = 1$) under the relevant boundary conditions, the Eq. (30) is solved and $U_0(R)$ is obtained as:

$$U_0(R) = \frac{2r^*[(r^{*2}-1)\ln R - (R^2-1)\ln r^*] + \frac{A_1}{1+r^*}\left[-R^2 + 2r^*\ln R + A_1(r^*-1) + A_3\right]}{r^* - r^{*3} + \frac{A_2}{2} + \frac{A_1}{1+r^*}\left[A_1(r^*-1) + A_4\right]} \tag{32}$$

where

$$A_1 = 4Kn\beta_v(r^{*2}-1), \qquad A_2 = 2r^*(1+r^{*2})\ln r^*, \qquad A_3 = 1 + r^{*3} - 2r^*\ln r^*$$

$$A_4 = \frac{A_2 - 2r^{*2}}{r^*-1}\ln r^* + \frac{r^{*2} - 4r^* + 1}{2(1+r^*)} \tag{33}$$

By using Eq. (32), the Eq. (31) is solved under the regarding boundary conditions to obtain at the dimensionless temperature profile ($\theta_0(R)$).

For every integer $n>0$, the n-order boundary value problem is given, namely:

$$\frac{1}{R}\frac{d}{dR}\left(R\frac{dU_n}{dR}\right) = -\frac{1}{4(1-r^*)^2}\theta_{n-1} - \frac{1}{4(1-r^*)^2}\zeta_n$$

$$U_n(r^*) = 2\beta_v Kn(1-r^*)\left.\frac{dU_n}{dR}\right|_{R=r^*}, \qquad U_n(1) = -2\beta_v Kn(1-r^*)\left.\frac{dU_n}{dR}\right|_{R=1}$$

$$\int_{r^*}^{1} U_n R dR = 0 \tag{34}$$

$$\frac{1}{R}\frac{d}{dR}\left(R\frac{d\theta_n}{dR}\right)=-Br\left(\sum_{j=0}^{n}\left(\frac{dU_j}{dR}\frac{dU_{n-j}}{dR}-\frac{2}{1-r^{*2}}\eta_j U_{n-j}\right)\right)+\frac{r_q+r^*}{(1-r^{*2})(1-r^*)}U_n$$

$$\left.\frac{d\theta_n}{dR}\right|_{R=r^*}=0 \quad , \quad \left.\frac{d\theta_n}{dR}\right|_{R=1}=0$$

$$\int_{r^*}^{1}\theta_n(R)RdR=0 \tag{35}$$

Using the regarding dimensionless velocity and temperature profiles, the dimensionless bulk temperature θ_b is given by:

$$\theta_b=\frac{T_b-T_m}{q_i''D_h/k}=\frac{\int_{r^*}^{1}U\theta RdR}{\int_{r^*}^{1}URdR}=\frac{2}{1-r^{*2}}\int_{r^*}^{1}U\theta RdR \tag{36}$$

The Nusselt number based on the difference between the wall and the fluid bulk temperature is given by:

$$Nu_i=\frac{-2(1-r^*)\left.\frac{d\theta}{dR}\right|_{R=r^*}}{\frac{T_1-T_b}{q_i''D_h/k}}=\frac{1}{\theta(r^*)-\theta_b+\beta_t Kn} \tag{37}$$

$$Nu_o=\frac{2(1-r^*)\left.\frac{d\theta}{dR}\right|_{R=1}}{\frac{T_o-T_b}{q_i''D_h/k}}=\frac{r_q}{\theta(1)-\theta_b+r_q\beta_t Kn} \tag{38}$$

For all the cases considered, the above sequential solution procedure is continued until the change in *Nu* values between two successive steps is negligible. The obtained results showed that including the first 4 terms is sufficient to for adequate accuracy.

3. RESULTS AND DISCUSSION

In this study, combined effects of mixed convection parameter and viscous dissipation on the fully developed laminar mixed convection flow of a rarefied gas inside a vertical micro-annulus are investigated theoretically by using the perturbation method. The channel walls are maintained at uniform constant heat flux thermal boundary condition and the viscous dissipation in the fluid is taken into account.

Br	*Kn = 0.00*		*Kn = 0.05*		*Kn = 0.10*	
	Present	Ref. [18]	Present	Ref.[18]	Present	Ref. [18]
0.00	8.2957	8.2950	5.3514	5.3511	3.8110	3.8117
0.02	7.3438	7.3367	5.2188	5.2192	3.7800	3.7803
0.04	6.5972	6.5702	5.0895	5.0936	3.7480	3.7494
0.06	5.9314	5.9432	4.9710	4.9739	3.7164	3.7191
0.08	5.4254	5.4208	4.8536	4.8597	3.6854	3.6892
0.10	5.0064	4.9787	4.7502	4.7505	3.6549	3.6599

Table 1. Comparison of *Nu* for present study and available results from Altunkaya et al. [18] for different values *Br* and *Kn* at $r^*\approx 0.98$, *Gr/Re=100*, r_q*=1* and *Pr=0.71*.

At first, we verified our analysis by comparing some limiting results with those available in the existing literature, mainly by those of Altunkaya et al. [18]. As it is seen from Table 1, comparison of our results with those in terms of the Nusselt number for different values of *Br* and *Kn* at *Gr/Re=100* and $r^*\approx 0.98$ showed a good agreement.

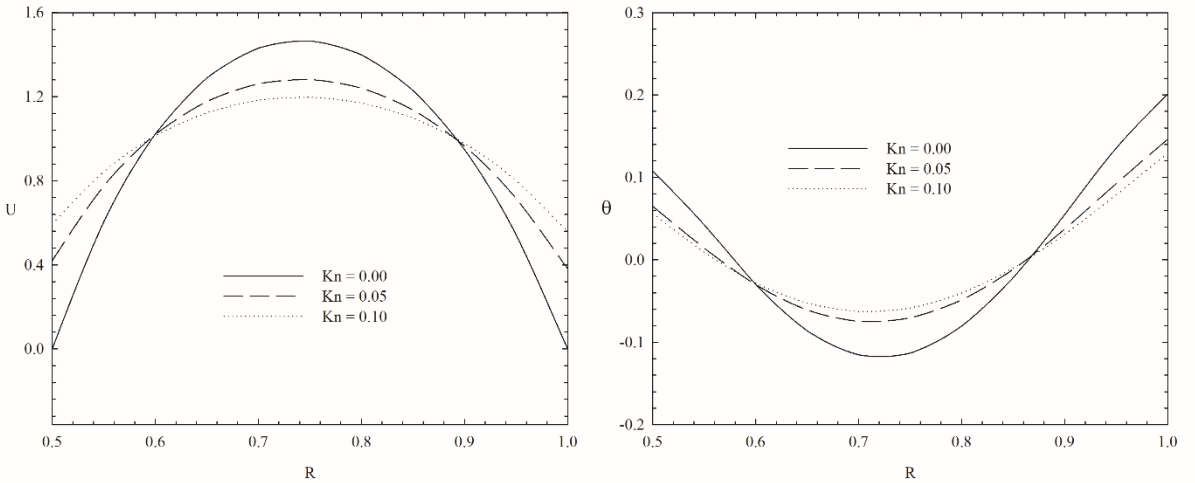

(a) (b)

Figure 2: The variation of dimensionless velocity (a) and dimensionless temperature (b) with R for different values of *Kn* at *Gr/Re=100*, r_q*=1 and Br=0.10*.

The variation of the dimensionless velocity and temperature with the ratio of wall heat flux for various values of the Knudsen number at *Gr/Re* = 100 and *Br* = 0.10 is given Fig. 2a and b, respectively. As it is seen from Fig. 2a, the fluid velocity in the vicinity of the wall increases with an increase in the Knudsen number while the maximum velocity decreases at the center of the channel. This behavior is attributed to the increase in the buoyancy forces and change in the momentum transfer at the wall as a result of different slip velocities.

A similar behavior is also obtained for the temperature distribution as the *Kn* number increases. As it is seen from the Fig. 2 b., the fluid temperature increases in the vicinity of the wall with an increase in the *Kn* number. Here, it should be noted that the definition of the dimensionless temperature is $\theta = {T - T_m}\big/{(q_i'' D_h / k)}$.

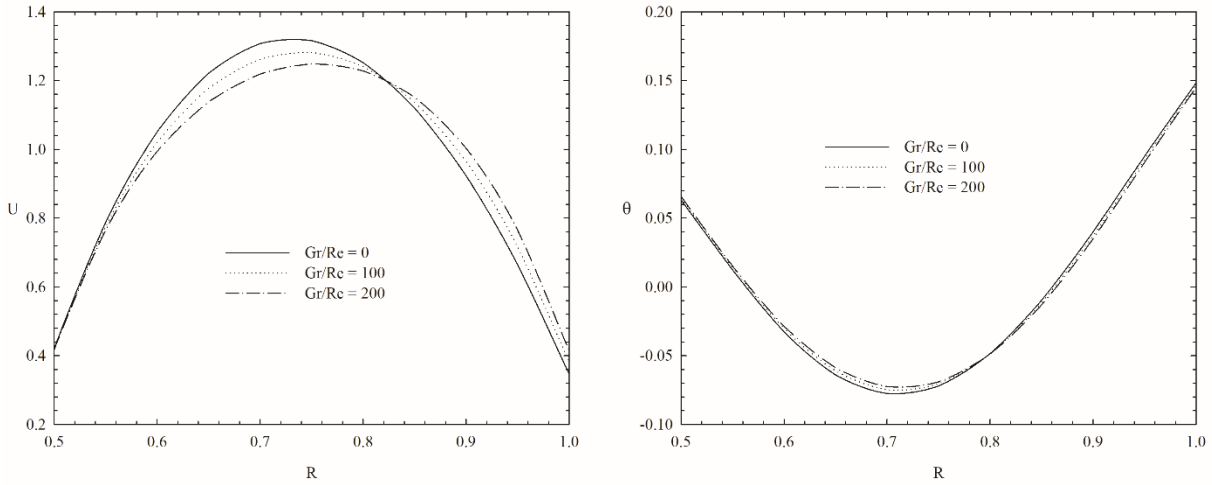

(a) (b)

Figure 3: The variation of dimensionless velocity (a) and dimensionless temperature (b) with R for different values of *Gr/Re at Kn=0.05*, r_q*=1 and Br=0.10*.

For *Kn=0.05* and *Br=0.10*, the effect of the mixed convection parameter on the dimensionless velocity and temperature profiles is given Fig. 3. Here, $Gr/\mathrm{Re} = 0$ and $Gr/\mathrm{Re} \neq 0$ represent the forced convection and the

mixed convection cases, respectively. Due to an increase in *Gr/Re* in the microannulus flow, the maximum velocity profile shifts towards outer wall. This behavior is the result of the contribution of fluid momentum in the region near the wall due to the high buoyancy forces (Fig. 3a).

In Figure 3b, with an increase in *Gr/Re*, it is seen that the dimensionless temperature exhibits an increasing tendency in the inner wall while a decreasing tendency in the outer wall.

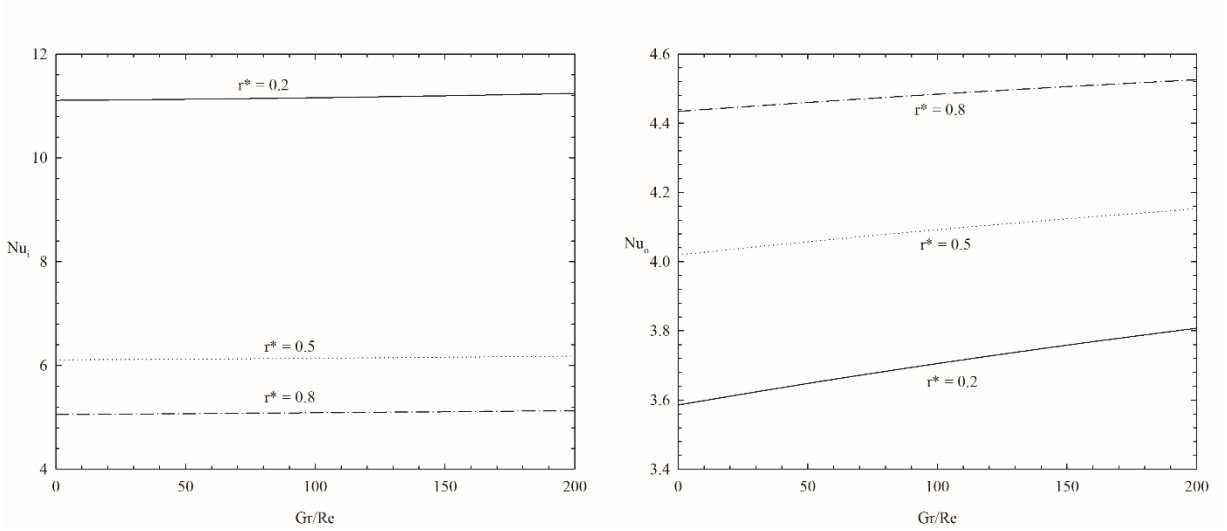

Figure 4: The effect on *r** on the variation of *Nu* with *Gr/Re* in the inner cylinder (a) and outer cylinder (b) *at.Kn=0.05, Br=0.1, r_q=1, Pr=0.71.*

The effect of *r** on the variation of *Nu* with *Gr/Re* is depicted in Fig. 4. As general behavior, for all the values of *Gr/Re*, the increase in *r** results in a decrease in the *Nu* at the inner wall while the opposite is true at the outer wall. For the both walls, the influence of the increasing *Gr/Re* is to increase the *Nu*. However, this *Nu*-dependence on *Gr/Re* is negligible for the inner wall.

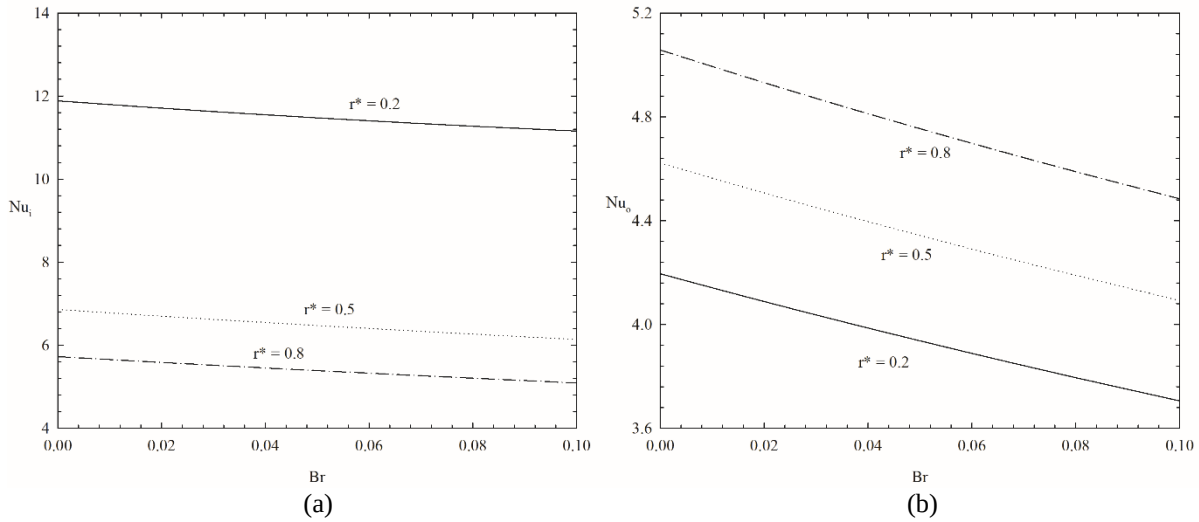

Figure 5: The effect on *r** on the variation of *Nu* with *Br* in the inner cylinder (a) and outer cylinder (b) *at Kn=0.05, Gr/Re=100, r_q=1, Pr=0.71.*

For *Gr/Re*=100 and *Pr*=0.71, Fig. 5 shows the effect *Br* on the *Nu* for various values of *r**. At both walls, it is seen that the *Nu* tends to decrease with an increase in *Br*. This behavior can be explained by the internal heating effect

of viscous dissipation which leads high wall temperatures. For a constant value of q_w'', it is clear that the increase in *Br* increases $T_w - T_b$ and consequently reduces the *Nu*.

4. CONCLUSIONS

In this study, the combined effects of mixed convection parameter and viscous dissipation on a fully developed laminar micro-annulus flow are investigated theoretically. The slip velocity and temperature jump conditions at the walls and the viscous dissipation in the fluid have been included in the analysis. The major findings can be summarized as follows:

1. The maximum velocity shifts towards outer wall with an increase in the mixed convection parameter (*Gr/Re*).

2. The dimensionless wall temperature increases with increasing *Kn* due to the high temperature jumps at the walls.

3. The *Nu* at the inner wall is nearly independent of *Gr/Re* while it increases at the outer wall with increasing with increasing *Gr/Re.*

4. The Nu at the inner wall get lower values with an increase in *r**, while the opposite is true at outer wall.

5. Either at the inner and outer wall the *Nu* decreases with increasing *Br*.

5. NOMENCLATURE

Br Brinkman number [$= \mu u_m^2 / q_i'' D_h$]
c_p specific heat at constant pressure [Jkg^{-1} K^{-1}]
C dimensionless parameter [$-\frac{Gr}{4\,\mathrm{Re}}(r_q + r^*)/((1-r^*)^4(1+r^*))$]
D_h hydraulic diameter [m]
g gravitational acceleration
Gr Grashof number [$= \beta g q_i'' D_h^4 / k\nu^2$]
h convective heat transfer coefficient [Wm^{-2} K^{-1}]
k thermal conductivity [Wm^{-1} K^{-1}]
Kn Knudsen number [λ / D_h]
Nu Nusselt number [$= hD_h / k$]
P dimensionless pressure [$= p / \rho u_m^2$]
Pr Prandtl number [$= \nu / \alpha$]
q'' heat flux [W/m^2]
r radial coordinate [m]
*r** ratio of radius [r_i / r_o]
r_q ratio of wall heat fluxes [q_0'' / q_i'']
R dimensionless radial coordinate [r / r_o]
Re Reynolds number [$= u_m D_h / \nu$]
T temperature [K]
T_m mean fluid temperature [K]
u axial velocity [m/s]
u_m mean velocity [m/s]
U dimensionless axial velocity [u / u_m]
x axial coordinate [m]

X dimensionless axial coordinate [$= x/\mathrm{Re}\, D_h$]

Greek symbols

α thermal diffusivity [$k/\left(\rho_0 c_p\right)$]

β_v, β_t dimensionless variables

γ specific heat ratio

ζ dimensionless pressure-drop parameter [$-dP/dX$]

η dimensionless parameter [$\int_{r^*}^{1} R\left(dU/dR\right)^2 dR$]

θ dimensionless temperature [$T - T_m \Big/ \left(q_i'' D_h/k\right)$]

λ molecular mean free path [m]

μ dynamic viscosity [Pa s]

ν kinematic viscosity [μ/ρ_0]

ρ_0 density [kg/m^3]

Subscripts

b bulk
i inner cylinder properties
m mean
o outer cylinder properties
s fluid properties on walls
w wall

6. REFERENCES

[1] Chen, C.K., & Weng, H.C. (2005). Natural convection in a vertical microchannel. *J. Heat Transfer*, 127, 1053-1056.
[2] Chen, C. K., & Weng, H. C. (2009). Drag reduction and heat transfer enhancement over a heated wall of a vertical annular microchannel. *Int. J. Heat Mass Transfer*, 52, 1075-1079.
[3] Haddad, O.M., Abuzaid, M.M., & Al-Nimr, M.A. (2005). Developing free convection gas flow in a vertical open-ended microchannel filled with porous media. *Numerical Heat Transfer Part A-Applications*, 48, 7, 693-710.
[4] Biswal, L., Som, S.K., & Chakraborty, S. (2007). Effects of entrance region transport processes on free convection slip flow in vertical microchannels with isothermally heated walls. *Int. J. Heat Mass Transfer*, 50, 1248-1254.
[5] Sadeghi, A., Asgarshamsi, A., & Saidi, M. H. (2010). Thermodynamic analysis of slip flow forced convection through a microannulus. *J. Thermophysics and Heat Transfer*, 24, 785-795.
[6] Rahimi, B., & Niazmand, H. (2014). Effects of high-order slip/jump, thermal creep, and variable thermophysical properties on natural convection in microchannels with constant wall heat fluxes. *Heat Transfer Eng*., 35, 1528-1538.
[7] Jha, B. K., Aina, B., & Isa, S. (2015). MHD natural convection flow in a vertical micro- concentric-annuli in the presence of radial magnetic field: an exact solution. *Ain Shams Engineering Journal*, 7, 1061-1068.
[8] Avci M., & Aydin O. (2007). Mixed convection in a vertical parallel plate microchannel. *J. Heat Transfer*, 129, 162-166.
[9] Avci M., & Aydin O. (2007). Mixed convection in a vertical parallel plate microchannel with asymmetric wall heat fluxes. *J. Heat Transfer*, 129, 1091-1095.
[10] Avci M., & Aydin O. (2009). Mixed convection in a vertical microannulus between two concentric microtubes. *J. Heat Transfer*, 131, 014502.
[11] Karimipour, A., Nezhad, A.H., D'Orazio, A., & Shirani, E. (2012). Investigation of the gravity effects on the mixed convection heat transfer in a microchannel using the lattice Boltzmann method. *Int. J. Therm. Science*, 54, 142-152.
[12] Jian, S.J., & Weng, H.C. (2013). Second-order mixed convective flow in a long vertical microchannel. *J. Heat Transfer*, 135, 022506.
[13] Sadeghi, A., Baghani, M., & Hassan, M. (2014). Gaseous slip flow mixed convection in vertical microducts with constant axial energy input. *J. Heat Transfer*, 136, (3), 032501.

[14] Sadeghi, M., Sadeghi, A., Saidi, A., & Hassan, M. (2014). Gaseous slip flow mixed convection in vertical microducts with constant but arbitrary geometry. *J. Thermophysics and Heat Transfer*, 28, (4), 771-784.
[15] Moslehi, M., & Saghafian, M. (2015). MHD mixed convection slip flow in a vertical microchannel heated at asymmetric and uniform heat flux. *Journal of Mechanical Science and Technology*, 29, 12, 5317-5324.
[16] Avramenko, A.A., Tyrinov, A.I., Shevchuk, I.V., Dmitrenko, N.P., Kravchuk, A.V., & Shevchuk, V.I. (2017). Mixed convection in a vertical circular microchannel. *International Journal of Thermal Sciences*, 121, 1-12.
[17] Jha, B. K., & Aina, B. (2018). Mixed convection flow in a vertical micro-annulus having temperature dependent viscosity: an exact solution. *Journal of Nanofluids*, 7, 1-8.
[18] Altunkaya A. N., Avci M., & Aydin O. (2017). Effects of viscous dissipation on mixed convection in a vertical parallel-plate microchannel with asymmetric uniform wall heat fluxes: The slip regime. *Int. J. Heat and Mass Transfer*, 111, 495-499.
[19] Aung, W., & Worku, G. (1986). Theory of fully developed, combined convection including flow reversal. *Journal of Heat Transfer-Transactions of the ASME*, 108, 485-488.
[20] Barletta, A., & Rossi di Schio, E. (2001). Effect of viscous dissipation on mixed convection heat transfer in a vertical tube with uniform wall heat flux, *Heat Mass Transfer*, 38, 129-140.
[21] Hinch, E. J. (1932). Perturbation methods. Cambridge University Press.
[22] Gad-el-Hak, M. (Ed.) (2001). The MEMS Handbook. CRC Press, New York.